Haptic Feedback of Membrane Puncture with an MR-Compatible Instrumented Needle and Electroactive Polymer Display

Jung Hwa Bae*, Amy Kyungwon Han*, Christopher J. Ploch, Bruce L. Daniel and Mark R. Cutkosky

***Abstract*— We present results of experiments with a haptic feedback device that imparts tangential deformations to the fingertips for displaying changes in force experienced by an MR-compatible optically-instrumented biopsy needle. The display is actuated using multiple layers of MR-compatible electroactive polymers stretched in a plastic frame. Users can use the device to sense events such as membrane puncture, as the needle is driven through a tissue phantom, with 98.9% reliability.**

I. Introduction

With the rapid growth of magnetic resonance (MR) imaging as a diagnostic tool, there is an increased desire to perform interventions, like targeted biopsy, under MR guidance [1]. However, the MR bore presents challenges, including difficult patient access due to the small bore size and severe restrictions on materials for MR-compatibility. In addition, most electronic components that involve electrical current flow are precluded.

Teleoperation systems seek to address the patient access problem by relaying sensed information (force, temperature, etc.) back to the physician. This information can be displayed visually [2], aurally [3] or haptically [4]. Among these modalities, haptics are promising because they can provide a natural perception of changes in force, tissue stiffness, and friction experienced at the tool/tissue interface. Here, we consider the forces experienced by a long, slender biopsy needle as it punctures a membrane deep within tissue.

In previous work, we presented an MR-compatible instrumented biopsy needle with three optical fibers embedded in grooves along the inner stylet [5]. The needle can detect events like membrane puncture more accurately than a force/torque sensor at the needle base because measured forces are not masked by friction along the length of the needle. We displayed these forces with a voice coil actuator, which is not MR-compatible.

To maintain an MR-compatible system, we present a new haptic display based on electroactive polymer (EAP) actuators. These are actuated by a high, nearly static voltage and have no metal parts. The display imparts tangential forces and small motions to the skin of the fingertips when a user holds the active pads (tactors) as seen in Fig. 1.

In the following sections, we briefly review relevant prior work and then present our haptic display design and subsequent user experiments focused on membrane puncture detection. While the EAP has diminished fidelity for displaying forces when compared with the voice coil actuator, it nonetheless provides users with a clear sensation of membrane puncture. We conclude with a discussion of the results and future work.

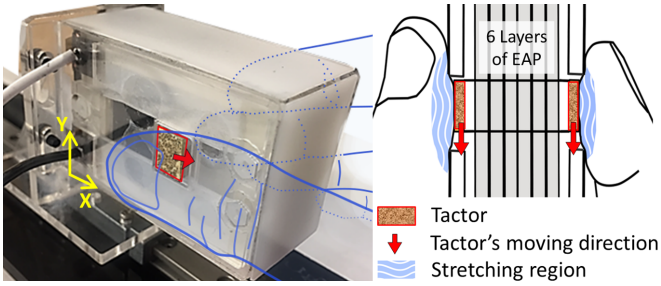

Fig. 1. Diagram of haptic display for tangential skin deformation in response to sensed changes in needle tip force. The x and y axes match with the ones in Fig. 2.

II. Related Prior Work

The related prior work includes robotic devices and instruments for MR-guided interventions and demonstrations of electroactive polymers as actuators for haptic applications.

Display of the forces required for needle insertion is beneficial for improving the ability of users to steer needles and detect membrane puncture [5]–[7]. A number of researchers present methods for instrumenting needles or catheters, some of which are MR-compatible [5], [8]. Various technologies have been proposed for actuating robots, teleoperators, and haptic devices for MR-guided procedures; see [9] for a recent review on percutaneous procedures. Hydraulics and pneumatics are common choices but are often bulky, bandwidth-limited, or lack stiffness [4], [10]–[12]. For small devices, ultrasonic piezoelectric motors can be designed with no ferromagnetic materials and very low electric currents [13]. However, they are inherently best suited as position-display devices as they are not backdrivable. We require a technology that is MR-compatible, compact, and capable of displaying a range of forces quickly.

Among the possible technologies, electroactive polymers (EAPs) are an attractive candidate. EAPs have been proposed for various applications, including haptic display [14]–[16], following their introduction nearly two decades ago [17], [18]. EAPs have also been demonstrated for applications requiring MR-compatibility with shielded cables and a power supply located outside the MRI room [19], [20]. Finally, because EAPs are light and compliant, they are suitable for low-power hand-held displays.

*J.H. Bae and A.K. Han contributed equally to the paper.

Bae, Han, Ploch and Cutkosky are in Mechanical Engineering and Daniel is in Radiology at Stanford University, Stanford, CA 94305, USA. jbae7 at stanford.edu, kwhan at stanford.edu

As actuators, EAPs have interesting properties in between those of ultrasonic motors and voice coil actuators: they are neither primarily displacement nor force sources. Rather, they are viscoelastic springs with varying force and stiffness as a function of the applied voltage. They can be matched to the requirements of a fingertip skin deformation display, which requires modest forces and moderate frequencies.

Skin stretch and skin deformation display are increasingly popular haptic modalities [21], [22]. Here, we consider deformation of the skin over the thumb and index finger pad in the proximal/distal direction (Fig. 1).

III. EAP Actuator Design

The electroactive polymer is a dielectric elastomer covered by stretchable electrodes on the upper and lower surfaces. When a large voltage is applied to the electrodes, the resulting Maxwell stress squeezes the elastomer's thickness, resulting in planar expansion. We use the same 3M VHB4910 film as in [18], [23], [24] for its high strain and toughness. This film is noticeably viscoelastic; applications that require small strains and higher frequencies often use a silicone rubber film instead.

The Maxwell stress can be represented as [18]:

$$\sigma = \varepsilon_0 \varepsilon_r E = \varepsilon (V/t)^2 \tag{1}$$

where ε_0 is the vacuum permittivity, ε_r is the relative permittivity, V is the applied voltage, and t is the thickness.

Performance in displacement- or force-producing applications depends greatly on the amount and direction of pre-stretch and how the film is mounted. In many applications, the best performance is obtained by applying a large ($\approx$ 400%) biaxial pre-stretch, which improves mechanical and electrical properties and reduces the film thickness from 1 mm to $< 70\mu$m [25].

A. EAP fabrication

A single EAP layer is shown in Fig. 2. After pre-stretching (Section III-B), the VHB film is supported by a 1 mm thick acrylic frame. It relaxes, and extends in the x direction when a voltage is applied. The electrodes are a thin layer of soft silicone rubber (Smooth-On Inc., Dragon Skin FX-Pro) saturated with carbon particles (FuelCellStore, Vulcan XC 72R) and thinned with toluene to a weight ratio of 9:1:26 (silicone:carbon:toluene). The electrodes are applied to the film through a mask. Connections to the electrodes are made with soft conductive fiber tape.

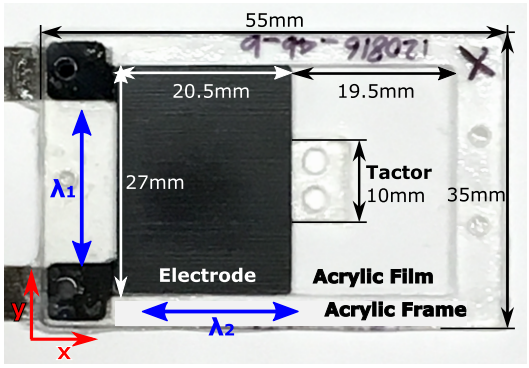

Fig. 2. A single layer of the EAP actuator; frame thickness $\approx$ 2mm.

B. Effect of pre-stretch

As noted earlier, the performance of the EAP using VHB4910 film depends on pre-stretch. In the present case, for uniaxial actuation against a human fingerpad with a stiffness of approximately 1.2 N/mm [26], the best results were obtained with a pre-stretch of 375% in the x direction and 400% in the y direction. Fig. 3 shows the results of several different pre-stretch ratios as different voltages are applied. The chosen solution produces less force at 5 kV, but exhibits a large strain and does not saturate, as the others do, for free displacements of 1 mm or greater. The pre-stretching process reduces the film thickness from 1 mm to 66.7μm.

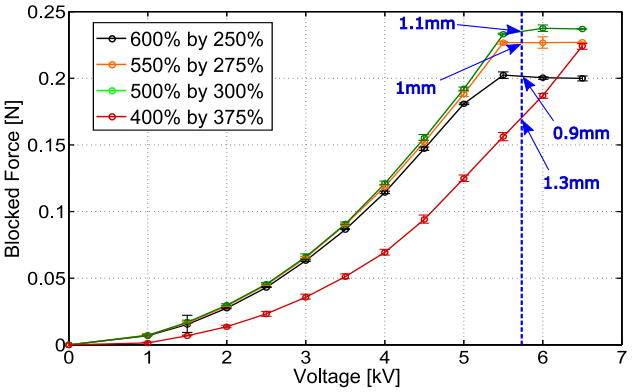

Fig. 3. Effect of pre-stretch ratio on performance. Force saturates at high voltage due to wrinkling. Free displacement at 5.75kV noted with blue font for each case. The 400% x 375% case produces less force, but does not saturate or wrinkle for displacements of 1 mm or greater. Final EAP design shown in Fig. 2 is 1.5 x wider than the specimens plotted here (18 mm film width), allowing free displacements up to 2.5 mm and larger forces (e.g., 0.26 N compared to 0.16 N at 5.5kV). The testing setup is explained in the following section.

C. Design requirements and final design selection

For the intended application, the haptic display must be light and sufficiently compact to hold and operate in-hand. Our device has a mass of 44 g and has dimensions of $6.2 \times 2.9 \times 3.8$ cm. Prior work on skin deformation displays [27] indicates that it is desirable to produce motions of 0.05-1 mm and forces of 0.1-2 N. To achieve motions and forces in the desired range we use six EAP layers in parallel and a film width of 27 mm and length of 40 mm giving a longer stroke (2.5 mm, 1.2 mm longer at 5.75 kV) and slightly higher forces (0.26 N, 0.1 N larger at 5.5 kV) than the specimens plotted in Fig. 3.

IV. Device Characterization

Figure 4 shows the apparatus used to test individual and multiple EAP layers. An acrylic rod connects the actuators to a muscle lever (Aurora Scientific, 309C) for controlled force/displacement trajectories. A benchtop high voltage supply (TREK, 610B) was used for the EAP characterization.

We are concerned primarily with the EAP performance when pressed against a human fingerpad. To estimate the expected performance, we conducted tests with the EAP

connected in series with a coil spring. The spring stiffness, at 1.2 N/mm, is similar to a lightly loaded human fingerpad in the proximal-distal direction [26]. Forces were measured with a load cell (ATI® Gamma) as seen in Fig. 4 B.

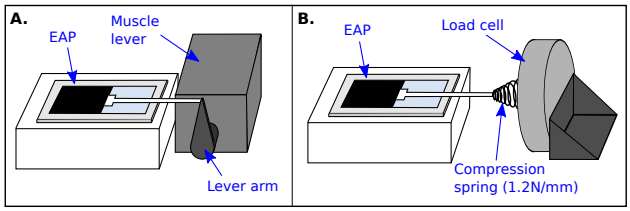

Fig. 4. Testing apparatus. (A) EAP film is connected to a muscle lever to measure force and displacement, (B) EAP is connected via a compression spring (1.2 N/mm) to a load cell to predict forces and motions when pressing against a human fingerpad.

A. Force and free displacement with a spring

As seen in Fig. 5, the force for a given voltage increases as we increase the number of EAP layers. The corresponding free displacement at maximum force, for 5.75 kV, is labeled.

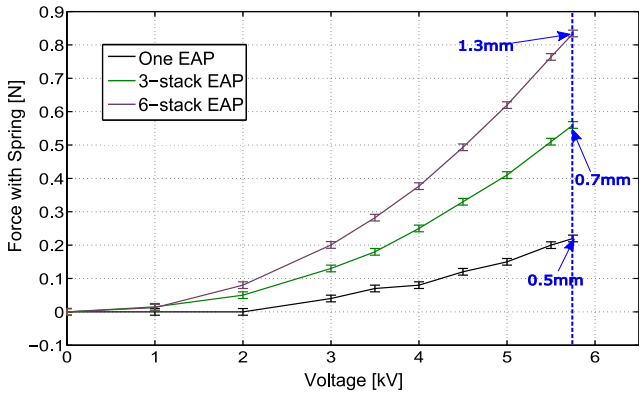

Fig. 5. Force with a spring in series for 1, 3 and 6 EAP layers. Free displacement is noted with blue font for each case at 5.75 kV.

B. Fore and displacement relationship

Although 1.2 N/mm is a reasonable baseline for human fingerpad stiffness, it varies considerably between subjects and depends on how firmly they hold the device. It is thus useful to characterize the force available at various deflections as a function of voltage (see Fig. 6). For each data point, the EAP was charged for 4 seconds at its initial (undeflected, blocked) position, held in place by the muscle lever. Then, the lever was moved in increments of 0.1 or 0.2 mm, and the force was measured at each position. As seen in the figure, the force/displacement behavior is approximately linear over the tested range of motion. For reference, the passive stiffness of the EAP in series with a 1.2 N/mm coil spring is also shown.

The information in Fig. 6 is useful to predict the variation in performance for different fingerpad stiffnesses. For example, (A) represents the case of a person with stiffer fingerpads, who experiences a somewhat higher force at lower displacement than person (B). Of course, the perception of skin stretch in either case depends on other factors as well so that the absolute threshold could be similar in both cases (Section VII-A.1).

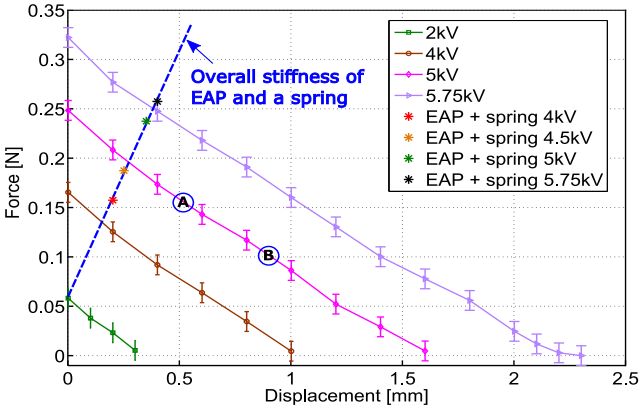

Fig. 6. Force and displacement relationship for a single EAP showing how force varies with fingerpad stiffness. Left intercept represents blocked force. Interaction force decreases with displacement. For 5kV, (A) represents an example of a person with stiff fingerpads, who experiences a higher force and smaller displacement than a person with softer fingerpads (B). Ascending line shows the combined stiffness of the actuator and coil spring for reference.

V. Haptic Feedback System

The haptic feedback system consisted of several communicating components, as shown in Fig. 7.

1) Force sensing needle: A force sensing needle based on fiber Bragg gratings (FBGs) [28] was used to measure tool-tissue interaction forces. It has four sets of FBGs distributed along the fibers, which are embedded in grooves in the inner stylet and hence not affected by friction from tissue on the needle. To improve temperature compensation, we used a set of FBGs near the base of needle to read the axial force.

2) Realtime control system: The optical interrogator (Micron Optics, SM-130) samples the FBGs at 1 kHz. The overall latency from when a force is applied to the needle to a commanded change at the output of the high voltage supply is approximately 50 ms.

3) High voltage control circuit for EAP actuation: EAP actuators require voltages higher than standard transistors tolerate so we built a switching circuit to charge and discharge the EAP actuators as shown in Fig. 8.

For the portability and easy integration of the haptic system, we used a high voltage amplifier (XP-EMCO, AH60) which produces up to 6 kV, linearly proportional to the input voltage of 0.5-5 V.

The high voltage opto-coupler (Voltage multiplier Inc., OC100G) and a high voltage resistor were used to limit the charging current for safety. The maximum current an opto-coupler can discharge is 120 μA and the current that can be supplied to an EAP from the charging opto-coupler is

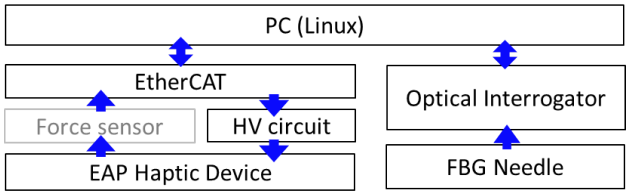

Fig. 7. System schematic block diagram. Force sensor was used only for characterizing the system.

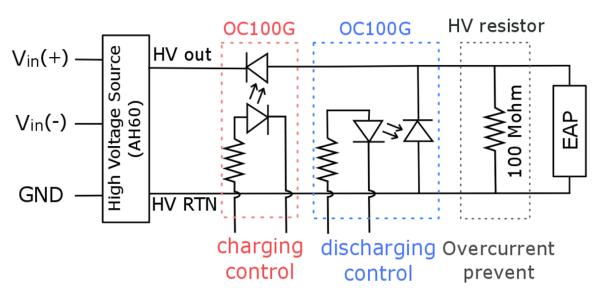

Fig. 8. The high voltage control circuit for the EAP device. The resistances of power resistors in the charging and discharging circuit is 600 Ω and 300 Ω, respectively.

60 μA. We grounded all user-contacting parts and limited the maximum supply current for user safety.

A 1000:1 high voltage differential probe (Keysight Technologies Inc., N2891A) was used for testing the circuit.

VI. Displaying Forces with EAP Actuators

The EAP actuator was connected in series with a 1.2 N/mm spring as in previous tests, and control signals were sent via the charging circuit. The discharging circuit is controlled by switching the opto-coupler. First, we compared the input control signal and EAP output force in response to a step function. The charging speed is faster than the discharging speed and there is some viscoelasticity in the VHB material. Thus, the initial response to a step function is considerably faster than the relaxation, as seen in Fig. 9.

Increasing the discharge rate of the EAP is useful to increase the responsiveness of the system to repeated forces. Combination of a 100 MΩ resistor in parallel with the EAP (which slightly reduces the maximum force) and an opto-coupler increased the discharge rate (Fig. 9).

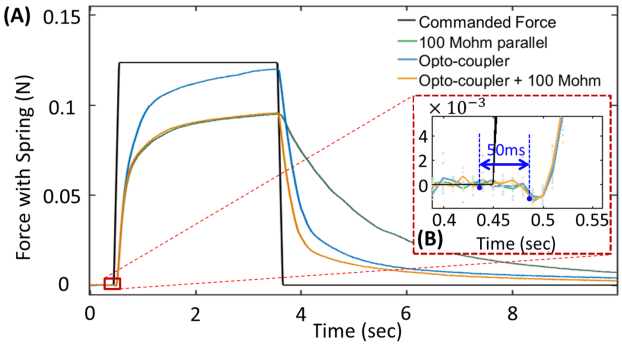

Fig. 9. (A) EAP (3-stack) force profile for 3 discharging methods with a step voltage command (force command) that rises over 0.1s, holds for 3s and falls over 0.1s. Solid curves show average values for a group of 5 tests. Enlarged view (B) shows the delay from the start of voltage rise to EAP response.

In addition, we extended, in software, the discharging period associated with each drop in force, producing the results shown in Fig. 10.

For an isolated event such as a membrane puncture, residual force due to slow discharging is not a limitation; however, for rendering continuous dynamic forces, this effect would be problematic. Furthermore, insufficient discharging may cause accumulation of residual charges and result in

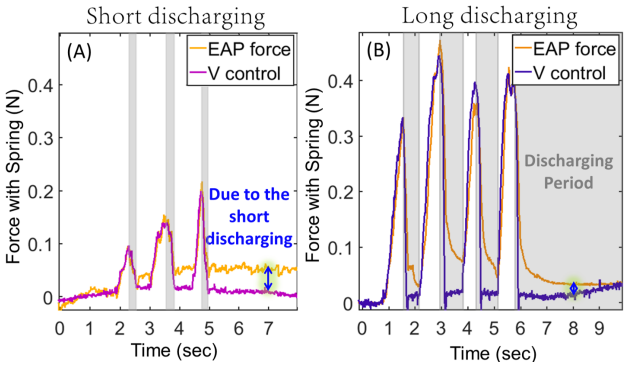

Fig. 10. Different discharging periods produce different results for a needle tapped on a rubber block in air.

shifting the baseline force, as seen in needle tapping data in Fig. 10 A. The grey area shows when the discharging opto-coupler is on. Fig. 10 B has a longer discharging period, thus charge does not accumulate.

VII. User Studies

Twelve test subjects (10 male, 2 female, age range: 23-33 years old; mean: 26.1 years old), all without medical experience in manipulating needles, were recruited for the experiments. We trained the subjects to have a similar grip force and asked them to maintain a consistent force for the experiments.

A. Absolute threshold test

To test the functionality of the EAP skin stretch device we first checked the absolute threshold and compared it to other skin stretch devices that use small RC servos or DC motors.

1) Method: A simple up-down staircase method was used to obtain the detection threshold (X_{50}) [29]. Data were collected until the 12th reversal, and analyzed as described in [29]. Stimuli were given at random time intervals to prevent users from predicting the timing. In operation, the skin stretch device's tactors move with pre-defined speed until they reach the target stimulus magnitude, remain for 2 seconds, and then return to the initial position at 1/6 the speed. Thresholds were obtained for speeds of 0.194 N/s, 0.439 N/s, and 0.930 N/s. In all cases, the initial stimulus was 0.11 N.

Force [control voltage]	**0.19 (N/s) [2 V/s]**	**0.44 (N/s) [3 V/s]**	**0.93 (N/s) [4 V/s]**
Mean	0.113 N	0.104 N	0.085 N
SD	0.018 N	0.012 N	0.009 N
Displacement (=F(N) / Finger pad stiffness)	**0.16 (mm/s)**	**0.37 (mm/s)**	**0.78 (mm/s)**
Mean	0.095 mm	0.086 mm	0.071 mm
SD	0.015 mm	0.010 mm	0.008 mm

TABLE I

Threshold of perceptible force results for 12 subjects

2) Results: The results summarized in Table I are consistent with prior research on skin stretch displays (e.g., [21], [27]), which report the absolute threshold that decreases as the speed of displacement increases.

B. Confusion matrix

To understand how well people can interpret the size of stimuli, we gave users 3 different magnitudes of force (and displacement). Excellent discrimination would give confidence that this device provides a useful representation of the tissue stiffness changes encountered during needle insertion.

1) Method: We chose the moving speed of stimulus as 0.6 N/s (0.5 mm/s, k = 1.2 N/mm), which approximates the slope of the peaks in the membrane puncture test with a constant insertion speed of 6 mm/s. Three stimulus magnitudes higher than the JND values were chosen from a pilot test: 0.15 N (small), 0.275 N (medium), and 0.5 N (large) (Fig. 11). Subjects received training until they were confident in differentiating the magnitudes. Each subject received 10 of each stimulus magnitude (30 total) in randomized order.

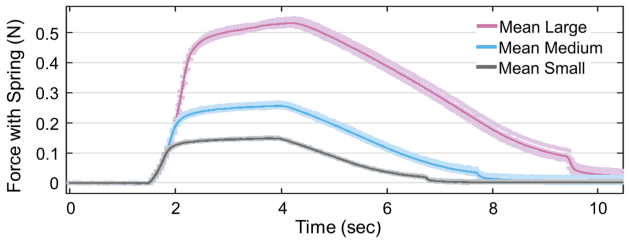

Fig. 11. EAP force output with a spring (k = 1.2 N/mm) corresponding to a small, medium and large stimuli. The slight increase in force over time is due to the viscoelasticity of the VHB film.

2) Results: Users differentiated small and large magnitudes well but often confused medium stimuli with small ones (23%) and large stimuli with medium ones (22%). Overall, users perceived the different magnitudes correctly with $> 70\%$ accuracy.

		Given		
		Small	**Medium**	**Large**
Answered	**Small**	**100 (83%)**	27 (23%)	0 (0%)
	Medium	19 (16%)	**84 (70%)**	26 (22%)
	Large	1 (1%)	9 (8%)	**94 (78%)**
Total		120	120	120

TABLE II

CONFUSION MATRIX FOR 12 SUBJECTS AND 10 INSTANCES OF EACH STIMULUS MAGNITUDE.

C. Membrane puncture detection experiment

1) Experiment Procedure: We approximated a robotic or teleoperated needle insertion system with a single-axis computer driven stage, to which the needle was attached (Fig. 12). As the stage drives the instrumented needle into a tissue phantom, the user manually tracks the needle motion by pushing the haptic device along a linear slide and feels for a membrane puncture. The tissue phantoms were gelatin, and the membranes were plastic film, 12.5μm thick. The gelatin stiffness was 8.3 kPa, corresponding to 325.6 N/m for the needle. Average membrane puncture forces were 1.01 N (SD = 0.01 N). For each phantom, a membrane was located at different locations: 3 cm, 6 cm, or 8 cm. The phantoms were used 6 times each in random order, resulting in 18 puncture tests. The phantom was covered with a curtain to prevent participants having visual feedback about the membrane puncture moment. Successful membrane puncture detection was defined as the user stopping the linear stage shortly after the needle punctures the membrane. The distance between the membrane and needle tip was measured with an encoder on the linear stage.

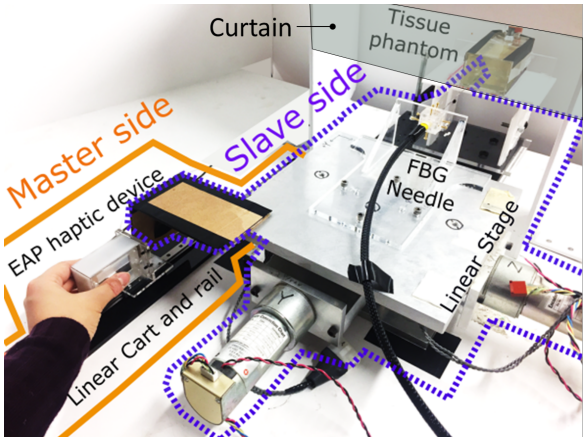

Fig. 12. "Teleoperation" system. The slave side is mounted on a linear stage that drives the FBG-instrumented needle into a tissue phantom. The axial needle tip forces it experiences are relayed to the master side and displayed with the EAP haptic device. The user's job is to manually track the slave side and feel for a membrane puncture.

2) Results: Users (N = 10) successfully detected 98.9% of membrane punctures, with the needle stopping an average of 4.5 mm after the membrane (SD = 1.6 mm). Much of this distance is due to various time delays in the system: First, there is at least 50 ms delay between the input control signal and the start of EAP actuation. Next, the user must perceive the change in the EAP haptic display. When the linear stage is moving at 6 mm/s, the force at the needle tip increases at 0.6 N/s due to the membrane stretching. From our JND study, we found that 0.104 N and 0.085 N is required for a constant display speed of 0.44 N/s and 0.93 N/s, respectively. Therefore, it takes between 91 ms (= 0.085 N / 0.93 N/s) and 236 ms (= 0.104 N / 0.44 N/s) to reach the threshold force with the speed of 0.6 N/s. The third step is the reaction time of a user to physically press the switch, which is approximately 367 ms with a standard deviation of 39 ms [30]. The last step is the mechanical time constant of the stage, which requires approximately 333 ms to come to a complete stop. Thus, in total, approximately 890 ms of time delay may occur between membrane puncture and needle stoppage. This time delay corresponds to 5.3 mm - displacement of the linear stage. Since our result 4.5 mm (SD = 1.6 mm) is comparable with the above calculation, we can conclude that the membrane puncture was detected successfully.

VIII. CONCLUSIONS AND FUTURE WORK

We presented a haptic device based on electroactive polymer films. The display provides tangential forces and displacements to a user's fingertips. It is small, light and

MR-compatible having no metal parts and negligible flowing current [19], [20]. To obtain forces and displacements consistent with the requirements of skin stretch displays, we used six pre-stretched EAP films in parallel. Although the film is viscoelastic, it responds rapidly to sudden increases in force, encountered in events like membrane puncture. To control the film, we developed a high voltage switching circuit using opto-couplers.

User tests determined the minimum perceivable stimulus, with results consistent with previous skin stretch devices (e.g., using small RC servos) as seen in Table I and II. In an application-oriented test, users were asked to track the motion of a needle inserted into a tissue phantom with a plastic "membrane" at an uncertain depth. The needle was instrumented with optical fibers to measure tip forces and monitored by an optical interrogator connected to a controller of EAP haptic device. Users were asked to press a button when they felt a stimulus corresponding to membrane puncture. They responded quickly and accurately in nearly all cases with an average response time of approximately 500 ms.

Future work will include improvements to the haptic device, increasing the mean time between failures of the EAP films. We will conduct further tests with subjects experienced in needle manipulation, and will verify that the entire system performs correctly with the needle inside an MR machine bore and the haptic display outside, nearby.

ACKNOWLEDGMENT

Special thanks to Xiyang Yeh for help in setting up the EtherCAT system. J.H. Bae is supported by the Kwanjeong Educational Fellowship, A.K. Han is supported by a Samsung Scholarship and C.J. Ploch is partially supported by Stanford CDR. Additional support was provided by NIH PO1 CA159992 and NIH SBIR R43-EB011822. User tests were conducted under Protocol IRB-26526.

REFERENCES

[1] N. V. Tsekos, A. Khanicheh, E. Christoforou, and C. Mavroidis, "Magnetic resonance-compatible robotic and mechatronics systems for image-guided interventions and rehabilitation: a review study." *Annu. Rev. Biomed. Eng.*, vol. 9, no. 1, pp. 351–387, 2007.

[2] J. Guo, E. Azimi, B. Gonenc, and I. Iordachita, "MRI-guided needle steering for targets in motion based on Fiber Bragg Grating sensors," in *2016 IEEE SENSORS*, vol. 9, no. 1. IEEE, 10 2016, pp. 1–3.

[3] A. Okamura, "Methods for haptic feedback in teleoperated robot-assisted surgery," *Industrial Robot: An Int. J.*, vol. 31, no. 6, pp. 499–508, 2004.

[4] W. Shang, H. Su, G. Li, and G. S. Fischer, "Teleoperation system with hybrid pneumatic-piezoelectric actuation for MRI-guided needle insertion with haptic feedback," in *IEEE IROS*, 2013, pp. 4092–4098.

[5] S. Elayaperumal, J. H. Bae, B. L. Daniel, and M. R. Cutkosky, "Detection of membrane puncture with haptic feedback using a tip-force sensing needle," in *IEEE IROS*, 2014, pp. 3975–3981.

[6] J. H. Bae, P. Christopher, L. Michael, B. L. Daniel, and M. R. Cutkosky, "Display of needle tip contact forces for steering guidance," *IEEE Haptics Symposium*, 2016.

[7] O. Gerovich, P. Marayong, and A. M. Okamura, "The effect of visual and haptic feedback on computer-assisted needle insertion," *Comput Aided Surg.*, vol. 9088, pp. 242–249, 2016.

[8] D. D. Lorenzo, Y. Koseki, E. D. Momi, K. Chinzei, and A. M. Okamura, "Coaxial needle insertion assistant with enhanced force feedback," *IEEE Trans Biomed Eng.*, vol. 60, no. 2, pp. 379–389, 2013.

[9] M. M. Arnolli, N. C. Hanumara, M. Franken, D. M. Brouwer, and I. A. M. J. Broeders, "An overview of systems for CT- and MRI-guided percutaneous needle placement in the thorax and abdomen," *Int. J. Med. Robot. Comput. Assist. Surg.*, vol. 11, pp. 458–475, 2015.

[10] N. Yu, W. Murr, A. Blickenstorfer, S. Kollias, and R. Riener, "An fMRI compatible haptic interface with pneumatic actuation," in *IEEE ICORR*, vol. 00, no. c, 2007, pp. 714–720.

[11] S. E. Song, N. B. Cho, G. Fischer, N. Hata, C. Tempany, G. Fichtinger, and I. Iordachita, "Development of a pneumatic robot for MRI-guided transperineal prostate biopsy and brachytherapy: New approaches," in *IEEE ICRA*, 2010, pp. 2580–2585.

[12] G. S. Fischer, I. Iordachita, C. Csoma, J. Tokuda, S. P. DiMaio, C. M. Tempany, N. Hata, and G. Fichtinger, "MRI-compatible pneumatic robot for transperineal prostate needle placement," *IEEE/ASME Transactions on Mechatronics*, vol. 13, no. 3, pp. 295–305, 2008.

[13] A. Erwin, M. K. O'Malley, D. Ress, and F. Sergi, "Development, Control, and MRI-Compatibility of the MR-SoftWrist," in *IEEE ICORR*, 2015, pp. 187–192.

[14] M. Y. Ozsecen, M. Sivak, and C. Mavroidis, "Haptic interfaces using dielectric electroactive polymers," in *Sensors and Smart Structures Technologies for Civil, Mechanical, and Aerospace Systems*, vol. 7647, no. 1, 2010, p. 764737.

[15] A. Mazzone, R. Zhang, and A. Kunz, "Novel actuators for haptic displays based on electroactive polymers," in *ACM VRST*, no. October, 2003, p. 196.

[16] D. De Rossi, F. Carpi, N. Carbonaro, A. Tognetti, and E. P. Scilingo, "Electroactive polymer patches for wearable haptic interfaces," in *IEEE EMBS*, no. Section III, 2011, pp. 8369–8372.

[17] R. Pelrine, R. Kornbluh, J. Joseph, R. Heydt, Q. Pei, and S. Chiba, "High-field deformation of elastomeric dielectrics for actuators," *Materials Science and Engineering C*, vol. 11, no. 2, pp. 89–100, 2000.

[18] R. Kornbluh, R. Pelrine, J. Joseph, Q. Pei, and S. Chiba, "Ultra-high strian response of elastomeric polymer dielectrics," in *Materials research society symposium*, vol. 600, 2000, pp. 119–130.

[19] J. Vogan, A. Wingert, S. Dubowsky, and M. Hafez, "Manipulation in M wises using Electrostrictive Polymer Actuators : ith an Application to Reconfig aging CO," in *IEEE ICRA*, 2004, pp. 2498–2504.

[20] F. Carpi, A. Khanicheh, C. Mavroidis, and D. De Rossi, "Silicone made contractile dielectric elastomer actuators inside 3-Tesla MRI environment," in *IEEE IROS*, 2008, pp. 137–142.

[21] C. J. Ploch, J. H. Bae, W. Ju, and M. Cutkosky, "Haptic skin stretch on a steering wheel for displaying preview information in autonomous cars," in *IEEE IROS*, 10 2016, pp. 60–65.

[22] Z. F. Quek, S. Member, S. B. Schorr, I. Nisky, A. M. Okamura, and W. R. Provancher, "Augmentation of stiffness perception with a 1-degree-of-freedom skin stretch device," *IEEE Trans. on Human-machine Sys.*, vol. 44, no. 6, pp. 1–12, 2014.

[23] R. Pelrine, R. Kornbluh, and G. Kofod, "High-strain actuator materials based on dielectric elastomers," *Advanced Materials*, vol. 12, no. 16, pp. 1223–1225, 2000.

[24] A. Orita and M. R. Cutkosky, "Scalable electroactive polymer for variable stiffness suspensions," in *IEEE/ASME Transactions on Mechatronics*, vol. 13, no. 9, 2015, pp. 2836–2846.

[25] G. Kofod, "The static actuation of dielectric elastomer actuators: how does pre-stretch improve actuation?" *J. of Phy. D: App. Phy.*, vol. 41, no. 21, p. 215405, 2008.

[26] N. Nakazawa, R. Ikeura, and H. Inooka, "Characteristics of human fingertips in the shearing direction." *Biological cybernetics*, vol. 82, no. 3, pp. 207–14, 2000.

[27] B. Gleeson, S. Horschel, and W. Provancher, "Design of a fingertip-mounted iactile display with iangential skin displacement feedback," *IEEE Transactions on Haptics*, vol. 3, no. 4, pp. 297–301, 2010.

[28] S. Elayaperurna, J. H. Bae, D. Christensen, M. R. Cutkosky, B. L. Daniel, R. J. Black, J. M. Costa, F. Faridian, and B. Moslehi, "Mr-compatible biopsy needle with enhanced tip force sensing," *WHC*, pp. 109–114, 4 2013.

[29] H. Levitt, "Transformed up- down methods in psychoacoustics," *JASA*, vol. 49, no. 2 pt 2, pp. 467–477, 1971.

[30] N. Hauthal, S. Debener, S. Rach, P. Sandmann, and J. D. Thorne, "Visuo-tactile interactions in the congenitally deaf: a behavioral and event-related potential study." *Frontiers in integrative neuroscience*, vol. 8, no. January, p. 98, 2014.